Supporting Information

Compact Aqueous Zinc-Carbon Capacitors with High Capacity and Ultra-long Lifespan

Yang Xu,[ad] Tao Li,[bc], Shicong Zhang,*[bc] ,Yi Shen,[bc] Fuqiang Huang*[b] and Tianquan Lin*[bc]

[a] State Key Laboratory of High-Performance Ceramics and Superfine Microstructure, Shanghai Institute of Ceramics, Chinese Academy of Sciences, Shanghai 200050, China

[b] School of Materials Science and Engineering, Shanghai Jiao Tong University, 800 Dongchuan RD, Shanghai 200240, China. Email: zhangshicong@sjtu.edu.cn; huangfq@sjtu.edu.cn; tqlin@sjtu.edu.cn

[c] Zhangjiang Institute for Advanced Study (ZIAS), Shanghai Jiao Tong University Shanghai 201210, China

[d] Center of Materials Science and Optoelectronics Engineering University of Chinese Academy of Sciences, Beijing 100049, China

*Corresponding authors: zhangshicong@sjtu.edu.cn (S. Z); huangfq@sjtu.edu.cn (F. H); tqlin@sjtu.edu.cn (T. L)

1. Experimental section

1.1 Materials

All reagents and materials in this work are commercially available and were used without further purification. 1,4-Dicyanobenzene ($C_8H_4N_2$, ≥ 98.0%) was purchased from Adamas-Beta (Shanghai, China). Zinc chloride ($ZnCl_2$, ≥ 98.0%) was purchased from Sigma-Aldrich. Zinc sulfate ($ZnSO_4 \cdot 7H_2O$, ≥ 99.0%), Hydrochloric acid (HCl, 36.0-38.0%), Ethanol (C_2H_6O, ≥ 99.5%) and Acetone (C_3H_6O, ≥ 99.5%) were purchased from Sinopharm Chemical Reagent Co., Ltd. Polytetrafluorethylene (PTFE, 60 wt% dispersion in H_2O) was purchased from Macklin (Shanghai, China).

1.2 Materials synthesis

Preparation of THC materials

The THC materials were synthesized by the ionothermal method.[1] Specifically, 1,4-Dicyanobenzene (1.00 g, 7.8 mmol) and anhydrous $ZnCl_2$ (5.32 g, 39.0 mmol) were mixed and transferred into a quartz ampule under Ar atmosphere. The ampoules were evacuated, sealed and heated at a specified temperature for 40 h. The obtained product was subsequently grounded and then washed with water to remove most of the $ZnCl_2$. Further stirring in 1 M HCl for 36 h was carried out to remove the residual $ZnCl_2$. After this purification step, the resulting powder was filtered, washed successively with

water, ethanol and acetone, and dried in vacuum at 90 °C overnight. The final products obtained were denoted as THC-XX (XX represents synthesis temperature, XX= 400, 500, 600 or 700).

Preparation of Precursor materials

To avoid carbonization, samples are also synthesized at 300 °C and 350 °C using the same synthesis method as THC materials (denoted as Precursor-300 and Precursor-350, respectively).

1.3 Material characterizations

X-ray diffraction patterns of THC materials powders were collected on a Bruker D8 Advance diffractometer equipped with mirror-monochromatic Cu Kα radiation (λ = 0.15406 nm). The FTIR spectra of THC materials were recorded by a Shimadzu IR Prestige-21 spectrometer. Raman spectra measurements of THC powders were taken on a LabRAM HR Evolution Raman microscope (HORIBA Scientific) under 532 nm laser irradiation. The measurement of N_2 adsorption/desorption isotherms was done by using a micrometrics ASAP 2460 system 77 K. The samples were degassed at 120°C for 12 h under a vacuum condition. The specific surface area was calculated by Brunauer-Emmett-Teller method. Temperature dependent conductivity was obtained from standard four-probe technique with the resistivity model and collected on physical properties measurement system (PPMS, Quantum Design). For the electric property tests, THC powders were pressed into square disc with silver paste as contact

electrodes.

1.4 Electrochemical Measurements

CR2016 coin cells were assembled to test the electrochemical properties. The THC electrodes were prepared by mixing the samples with acetylene black and PTFE with a weight ratio of 7:2:2 in isopropanol, respectively. The mixture was stirred and rolled into a free-standing film and dried at 90 °C for 3 h. Then, the film was cut into 6 mm discs and pressed onto titanium mesh (100 mesh). The loading mass of each electrode was 2-3 mg cm^{-2}. Zn foil (thick ness: 50 μm) was applied as both reference and counter electrode, glass fiber filter (GF/C, Whatman) as separator and 2 M $ZnSO_4$ as electrolyte. High-load electrodes (7-12 mg cm^{-2}) were also prepared using the same method. The rate and cycling tests were recorded using a Land BT2000 battery test system (Wuhan) at room temperature. Electrochemical impedance spectra were obtained from an electrochemical workstation (Autolab PGSTAT 302N, Switzerland) from 0.01 Hz to 100 kHz. The CV tests were recorded using CHI760 electrochemical workstation.

Figure S1. Powder photographs of (a) 1,4-dicyanobenzene, (b) precursor-300, (c) precursor-350, (d) THC-400, (e) THC-500, (f) THC-600 and (g) THC-700. Figure S1e also shows photographs of a black monolith (composed of THC-500 and $ZnCl_2$) obtained from in situ rearrangement of CTF precursor.

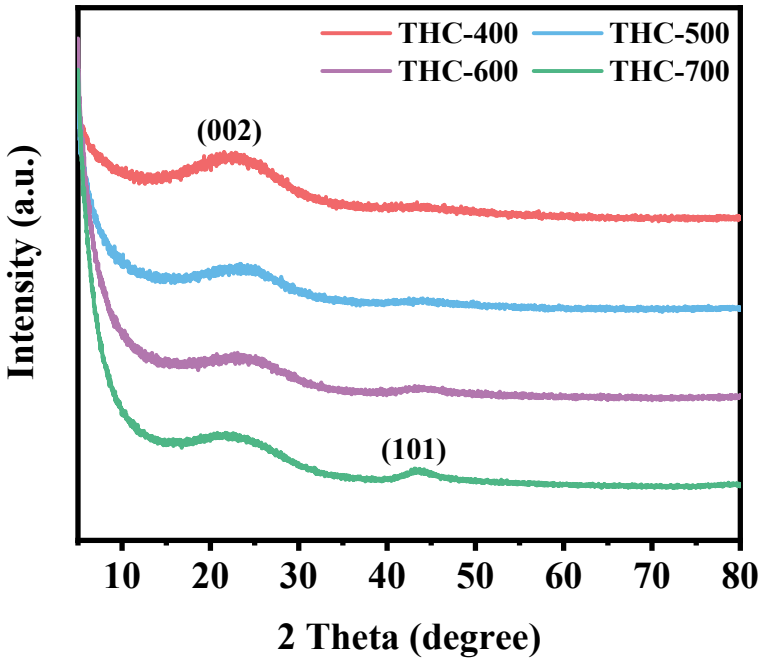

Figure S2. The XRD patterns of THC materials.

The pattern of THC-700 exhibit a new broad and weak hump which correspond to the (101) plane of graphitic carbon,[2] attributing to the large number of graphite microcrystals formed by the structural rearrangement of the benzene ring at high temperatures.

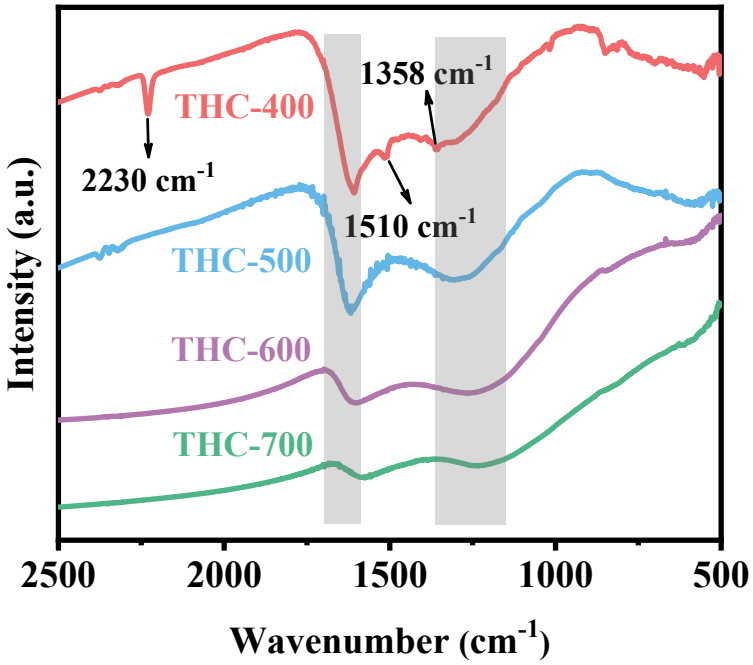

Figure S3. FTIR spectra of THC materials.

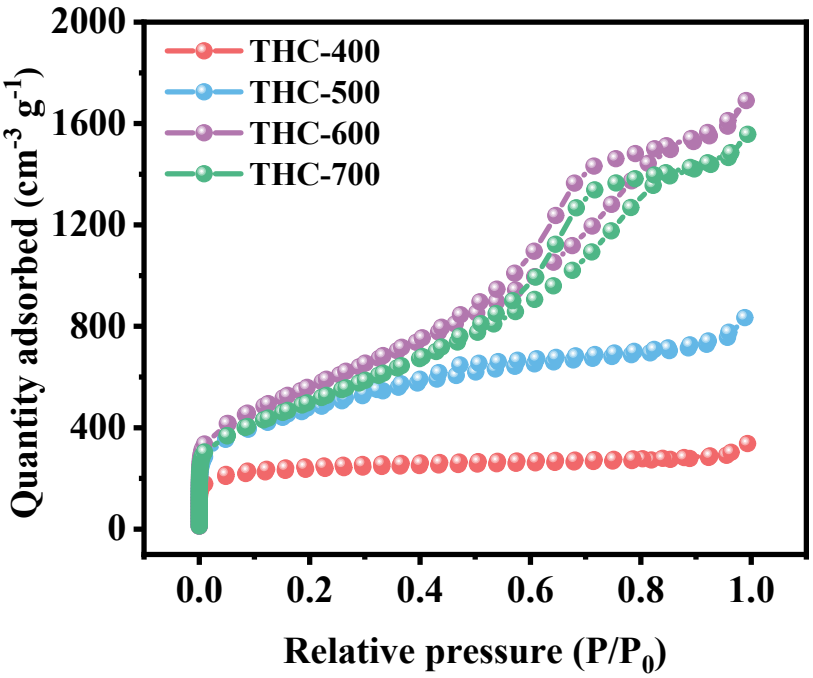

Figure S4. N_2 adsorption/desorption isotherms of THC materials.

Table S1. Pore structure parameters of THC materials.

Sample	SSA ($m^2\ g^{-1}$)	V_{total} ($cm^3\ g^{-1}$)	V_{micro} ($cm^3\ g^{-1}$)	V_{meso} ($cm^3\ g^{-1}$)	V_{meso}/V_{total} (a.u.)
THC-400	746	0.483	0.394	0.089	0.184
THC-500	1,650	1.17	0.532	0.638	0.545
THC-600	2,036	2.40	0.568	1.832	0.763
THC-700	1,837	2.23	0.517	1.713	0.768

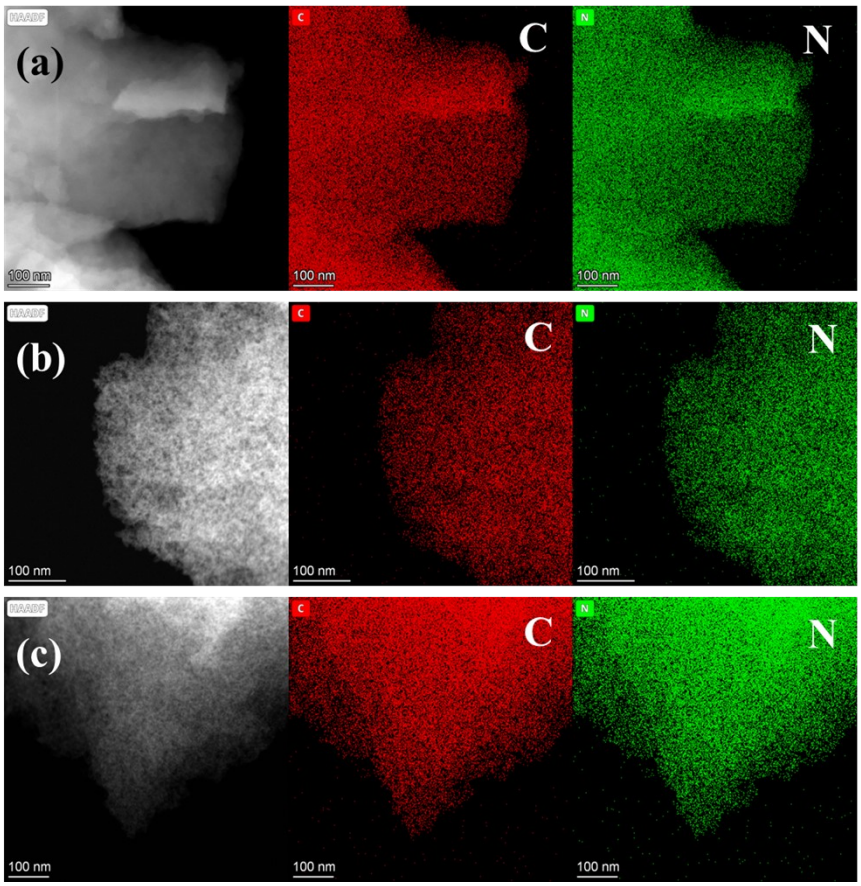

Figure S5. HAADF-STEM images and corresponding elemental mappings of (a) THC-400, (b) THC-600 and (c) THC-700.

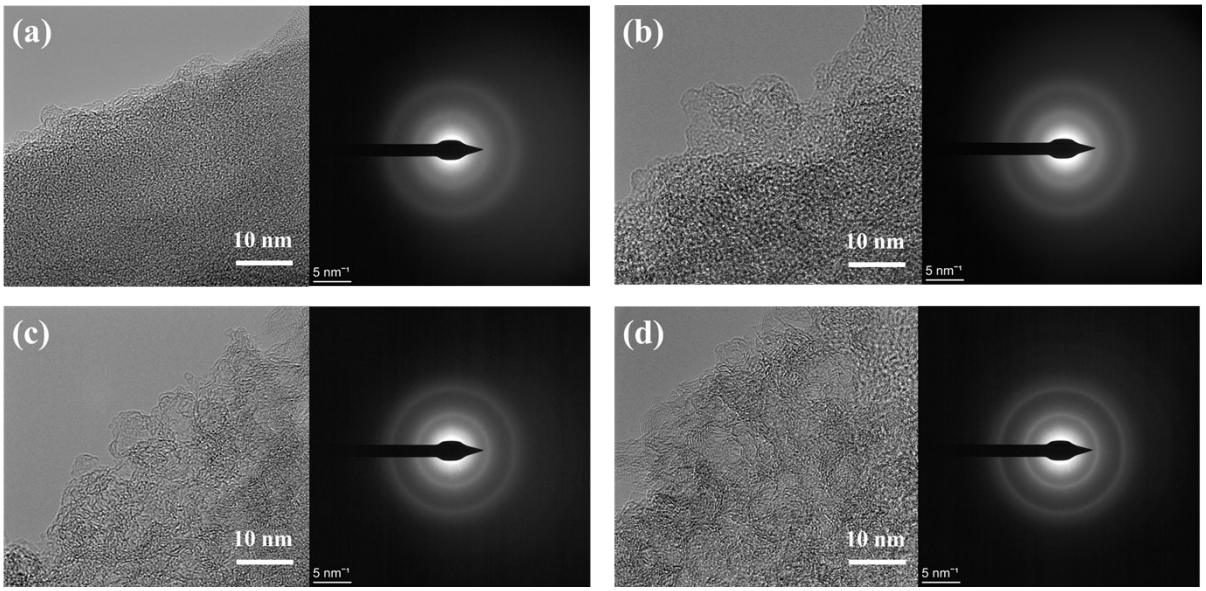

Figure S6. HRTEM images and relevant SAED patterns of (a) THC-400, (b) THC-500, (c) THC-600 and (d) THC-700.

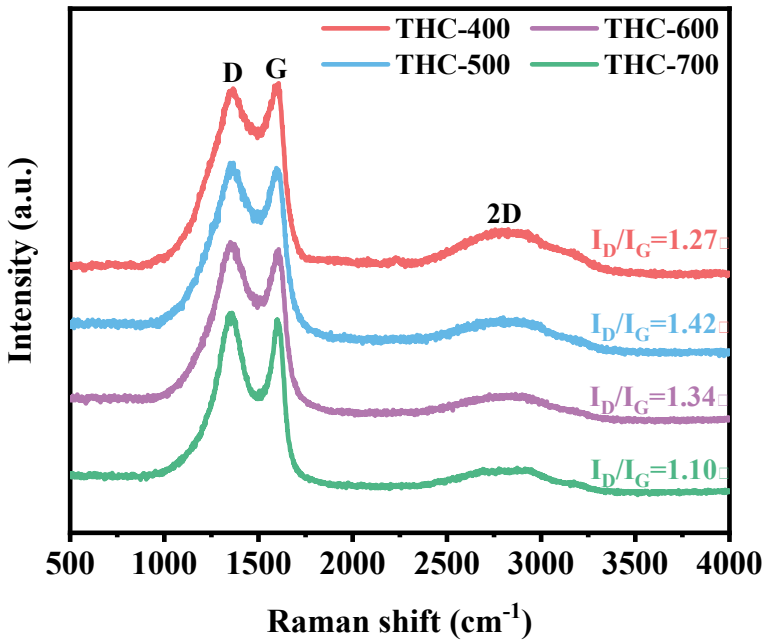

Figure S7. Raman spectra of THC materials.

It can be seen from Raman spectra that THC materials exhibit strong D-band (~1,350 cm^{-1}) and G-band (~1,580 cm^{-1}), induced by defects and graphitic structure, respectively. The intensity ratio (I_D/I_G) of the D-band and G-band can be used to assess the degree of carbon materials disorder.[3, 4] The I_D/I_G of THC-500 is 1.42, which is higher than 1.27 of THC-400, attributing to the structural rearrangement of the framework precursor. This leads to an increase in disorder. At higher temperatures, the I_D/I_G decreases to 1.34 of THC-600 and then decreases to 1.10 of THC-700, which is caused by a large number of graphite microcrystals formed by the rearrangement of the skeleton benzene ring under thermal driving.

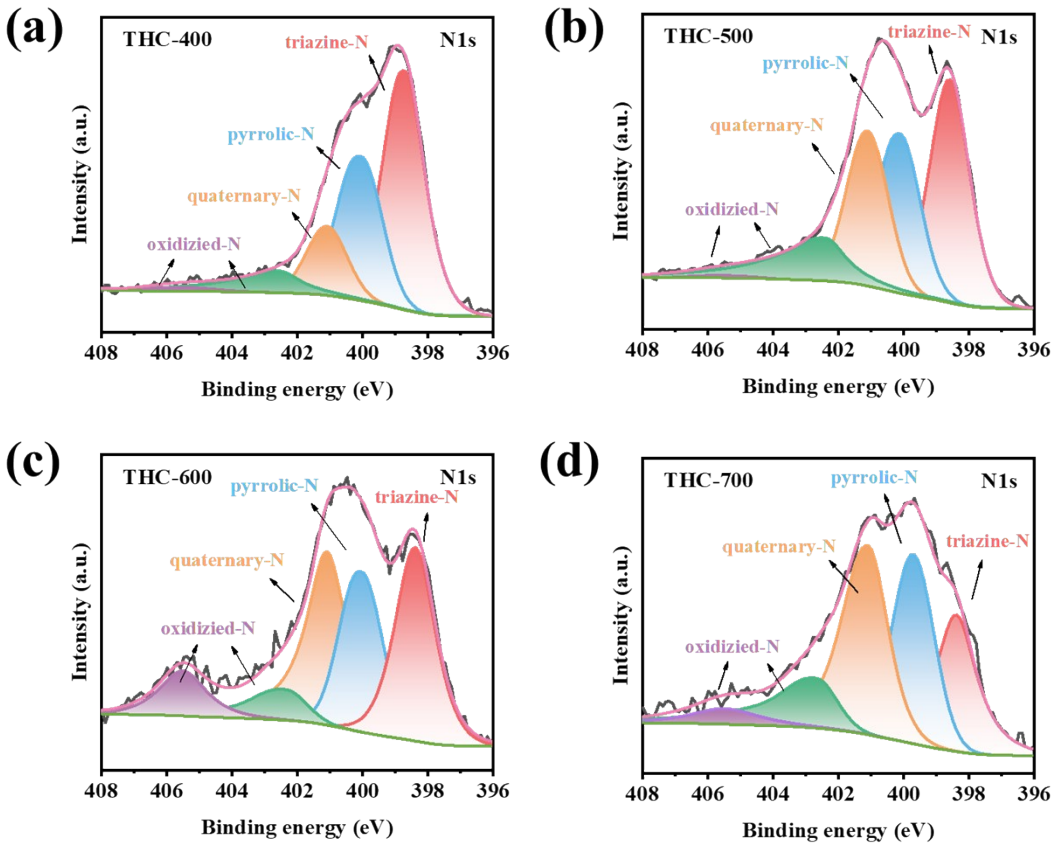

Figure S8. The high-resolution XPS spectra of N 1s of THC materials.

The high-resolution XPS spectra of N 1s can be deconvoluted into five peaks, including triazine/pyridine-N (~398.5 eV), pyrrolic-N (~400.0 eV), quaternary-N (~401.1 eV) and oxidizied-N (~402.4 eV and ~405.5 eV).[5-8]

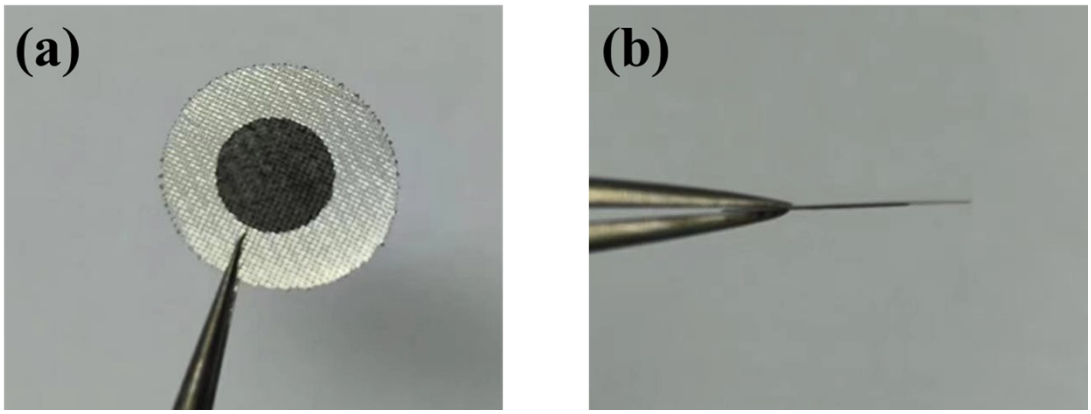

Figure S9. Photographs of THC electrodes.

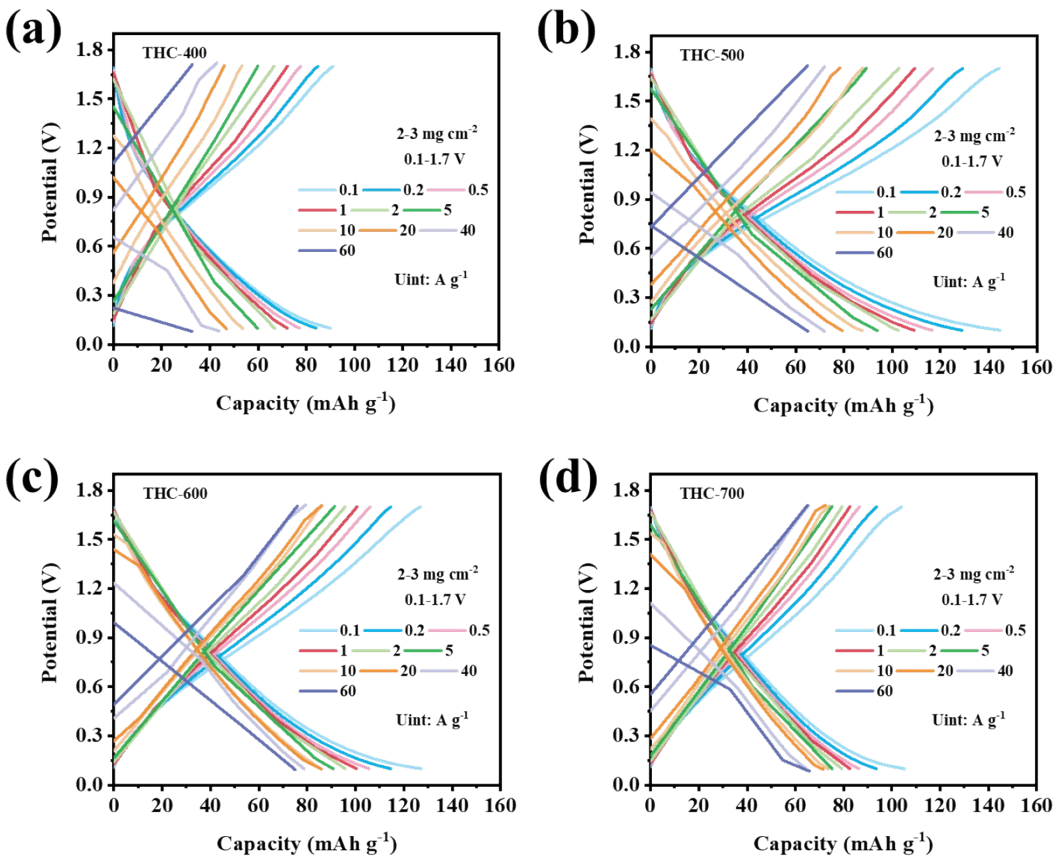

Figure S10. The GCD curves of (a) THC-400, (b) THC-500, (c) THC-600 and (d) THC-700 electrodes (with mass loading of 2-3 mg cm^{-2}) at different rates in the voltage range of 0.1-1.7V.

The reversible capacity of THC-400 is only 90 mAh g^{-1} at 0.1 A g^{-1}. With the increase of reaction temperature, the specific capacity of the THC-500 has been greatly increased, reaching 145 mAh g^{-1} at 0.1 A g^{-1}. Compared to THC-400, THC-500 has a considerable N/C ratio (0.122) and edge-N ratio (61%). The rich defect and higher carbonization degree promote the rapid transmission of electrons around the adsorption sites and activate more charge storage. Although THC-700 shows

a high electronic conductivity, it only provides 105 mAh g^{-1} at 0.1 A g^{-1}. This is due to the fact that higher reaction temperatures lead to a significant loss of edge-N.

The high rate of material depends on the rapid electron and ion transport at the bulk phase and surface interface.[9, 10] The capacity of THC-400, THC-500, THC-600 and THC-700 at 0.1 A g^{-1} are 90, 145 mAh g^{-1}, 126 mAh g^{-1} and 105 mAh g^{-1}, respectively. When the current density is increased to 40 A g^{-1}, the four provide capacity of 42 mAh g^{-1}, 72 mAh g^{-1}, 78 mAh g^{-1} and 66 mAh g^{-1}, respectively. Note that compared to THC-500, THC-600 displays better high-rate performance but lower capacity at low rates (only 126 mAh g^{-1} at 0.1 A g^{-1}). Considering the solvation effect of Zn^{2+} in the aqueous electrolyte ($[Zn^{2+}(H_2O)_6]$ possesses a hydration size of less than 1 nm), the micropores (<1 nm) supply multitudinous Zn^{2+} storage sites, whereas the mesopore and macropores act as rapid conduits for ion transportation, with minimal impact on electrochemical capacity.[9-11] In THC materials, the micropores originate from the intrinsic structure of covalent triazine frameworks, while the mesopores and macropores are formed by the connection of micropores during the thermal-driveled structure rearrangement process. Compared to THC-600, THC-500 inherits more intrinsic micropores from the covalent triazine framework, resulting in a higher capacity; In other words, for THC-600, a more sufficient thermal-driveled structure rearrangement sacrifices massive micropores, while forms more mesopores and macropores, resulting in relatively better high-rate performance. The two materials obtained by regulating the level of thermal drive, energy-oriented THC-500 and power-oriented THC-600, can be applied to different scenarios. Specifically, THC-500 exhibits the highest capacity output and decent high-rate performance. We selected the energy-oriented THC-500 for follow-up research.

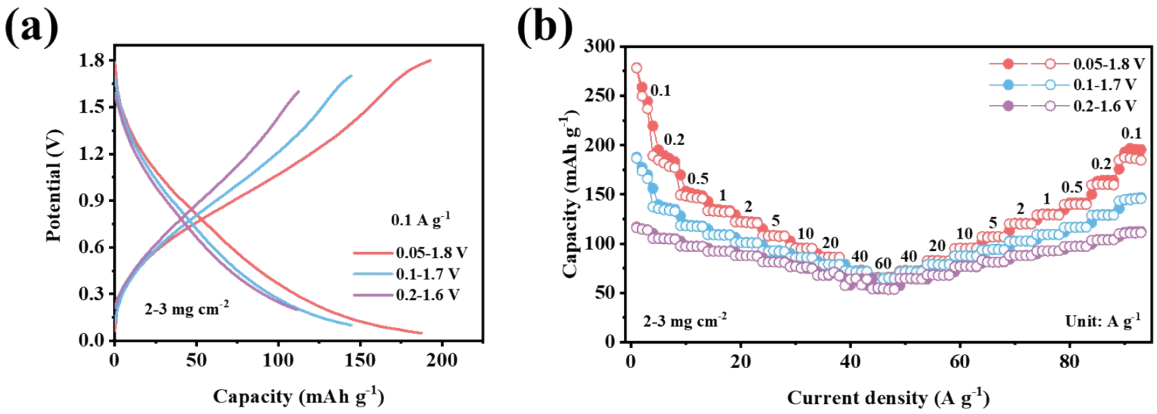

Figure S11. (a) Galvanostatic charge-discharge curves of THC-500 at 0.1 A g^{-1} in several voltage ranges; (b) Rate performance of THC-500 in several voltage ranges. The mass load of the THC electrodes tested above are 2-3 mg cm^{-2}.

Table S2. Comparison between the THC-500 and reported carbon materials in terms of capacity and rate performance.

Ref	Mass loading (mg cm^{-2})	Electrolyte	Voltage (V)	Capacity/Current density (mAh g^{-1}/A g^{-1})
THC-500	**2-3**	**2 M $ZnSO_4$**	**0.05-1.8** **0.1-1.7**	**187/0.1; 107/5; 83/20** **145/0.1; 94/5; 79/20**
SN-PCNTs[12]	0.7-0.8	2 M $ZnSO_4$	0.2-1.8	152.6/0.2; 80.6/5; 44.5/40
WC-6ZnN-12U[13]	6	2 M $ZnSO_4$	0.2-1.8	110/0.1; 82.3/0.5; 63.9/3
NPC[14]	1.5	1 M $ZnSO_4$	0-1.8	136.2/0.3; 69.2/15
rGO-200[15]	1.2-1.5	1 M $ZnSO_4$	0.01-1.8	121.8/0.5; 64.6/20
NLPC[16]	/	1 M $ZnSO_4$	0.1-1.8	85.5/0.1; 44.4/10
HPCS-900[17]	0.7-0.8	3 M $ZnSO_4$	0.1-1.7	104.9/0.1; 40.2/20
ORC[18]	2-3	1 M $ZnSO_4$	0.2-1.8	136.9/0.5; 85.8/10; 72/50
CT/SWNT-30[19]	2.7	1 M $ZnSO_4$	0.2-1.8	127.6/0.1; 72.4/20
AC[20]	0.7-0.8	2 M $ZnSO_4$	0.2-1.8	121/0.1; 41/20
Ca-900[21]	/	1 M $ZnSO_4$	0-1.8	~100/0.1; ~50/2
NPG[22]	~1.5	1 M $ZnSO_4$	0-1.8	105.1/0.5; 53.6/5
OPCNF-20[23]	0.9-1.2	1 M $ZnSO_4$	0.2-1.8	136.4/0.1; 38.8/20
OPC[24]	0.8-1.2	$ZnSO_4$ gel	0.2-1.8	132.7/0.2; 54.5/4
CNPK[25]	1.7-2.2	1 M $ZnSO_4$	0.2-1.8	103.2/0.1; 52.8/20
LDC[26]	2	1 M $ZnSO_4$	0.2-1.8	127.7/0.5; 42.8/20

GH film[27]	~2.5	2 M $ZnSO_4$	0.2-1.8	99.3/0.2; 60/10

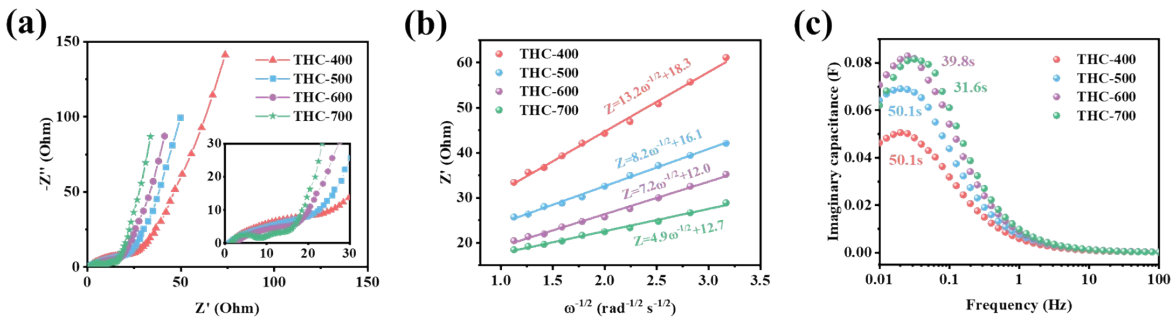

Figure S12. (a) Nyquist plots of THC materials; (b) relationship between the real part of impedance and low frequencies; (c) imaginary capacitance plots of THC materials.

The ion diffusion dynamics can be reflected by the linear relationship in the low frequency region according to the following equation: $\omega=2\pi f$ and $Z=R+\sigma\omega^{-1/2}$, of which ω represents angular frequency, f represents frequency, Z is the real part of impedance and σ is Warburg coefficient.[28, 29] Smaller σ value means faster ion transport during the electrochemical process. The reciprocal of the frequency at the maximum point in the imaginary capacitance plots, that is, the relaxation time constant (τ), reflects the temporal duration demanded to efficiently deliver the stored energy and power.[16, 30]

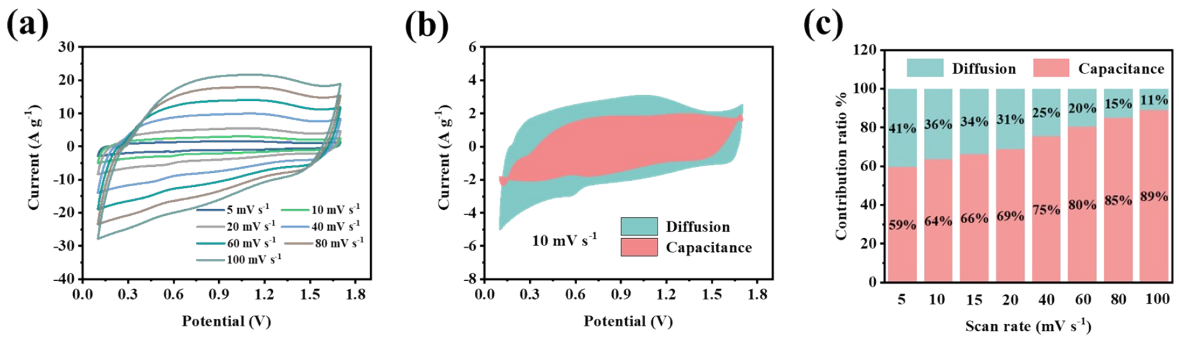

Figure S13. (a) CV curves of THC-500 at various scan rates; (b) capacitive and diffusion-controlled contributions at 10 mV s^{-1} of THC-500; (c) Normalized contribution ratio of capacitive and diffusion-controlled contributions at various scan rates of THC-500.

The total reaction current can be divided into diffusion current and capacitance current and described by the equation $i(v) = k_1v + k_2v^{1/2}$, where k_1 and k_2 stand for the capacitive and diffusion-controlled contributions in the energy storage process, respectively.[31]

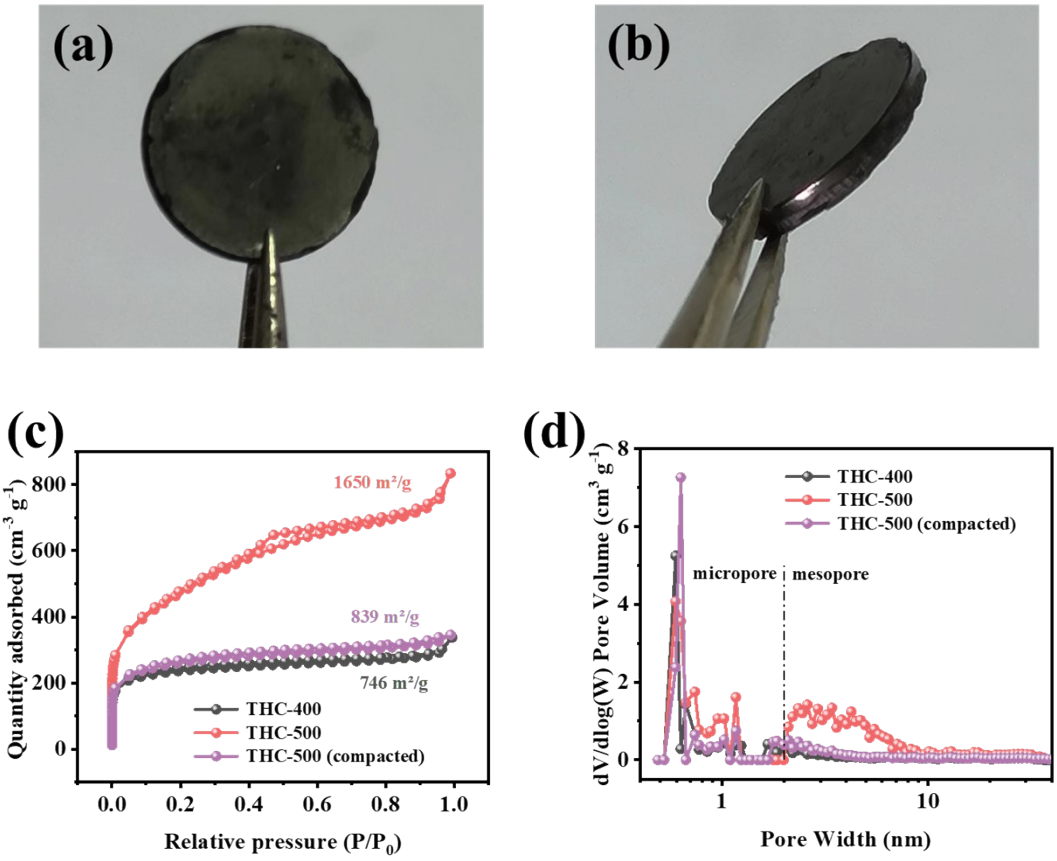

Figure S14. (a-b) Photographs of THC-500 (compacted); (c) N_2 adsorption/desorption isotherms and (d) pore size distribution of THC-400, THC-500 and THC-500 (compacted). THC-500 (compacted) was obtained by pressing powder into square disc (at 25 MPa).

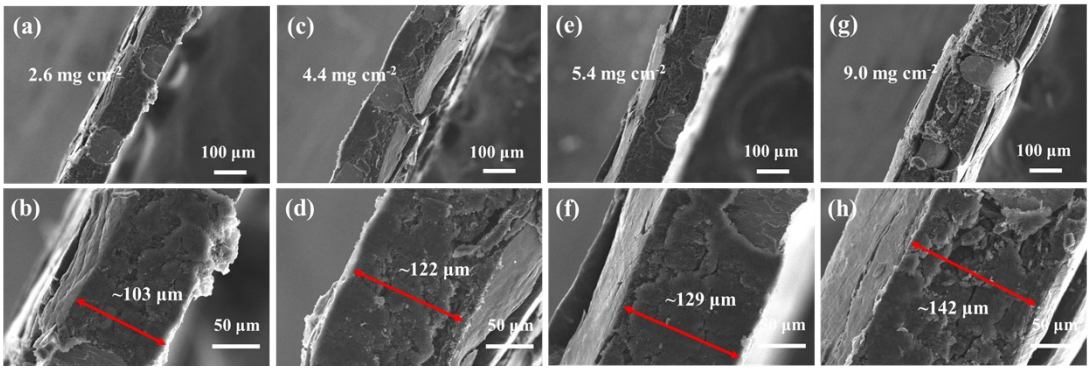

Figure S15. SEM images of electrode with different mass loading, and the thickness is marked by red lines.

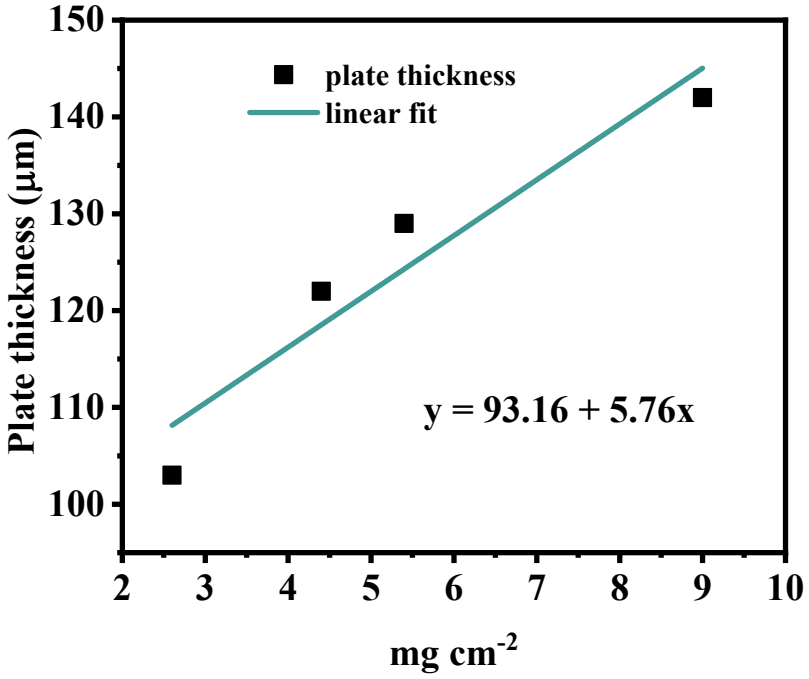

Figure S16. Relationship between the mass loading and thickness (obtained by fitting the data in **Figure S15**).

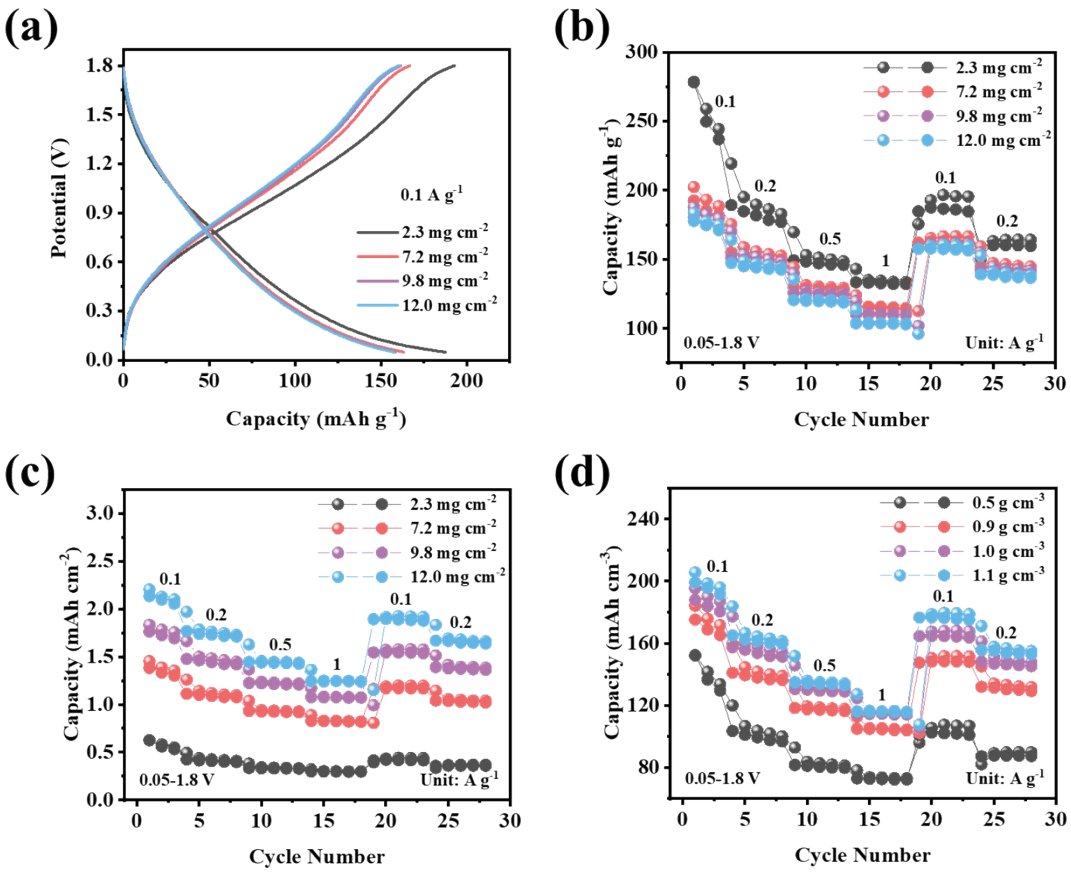

Figure S17. (a) Galvanostatic charge-discharge curves and (b-d) rate performance testing of THC-500 with different mass loadings.

The above high load electrodes are tested at 0.05-1.8 V (V vs Zn/Zn^{2+}). The average mass of 6 mm discs titanium mesh is 7.1 mg. According to the density of titanium (4.5 mg cm^{-3}), the volume of 6 mm discs titanium mesh is about 1.574×10^{-3} cm^3. The mass loading of the four electrodes is 2.3, 7.2, 9.8 and 12.0 mg cm^{-2}, respectively. The electrode thickness calculated according to the linear fitting equation of **Figure S16** is 106, 135, 149 and 162 μm, respectively. After deducting the volume

of titanium mesh, the density of the high load electrodes is 0.5, 0.9, 1.0 and 1.1 g cm^{-3}, respectively.

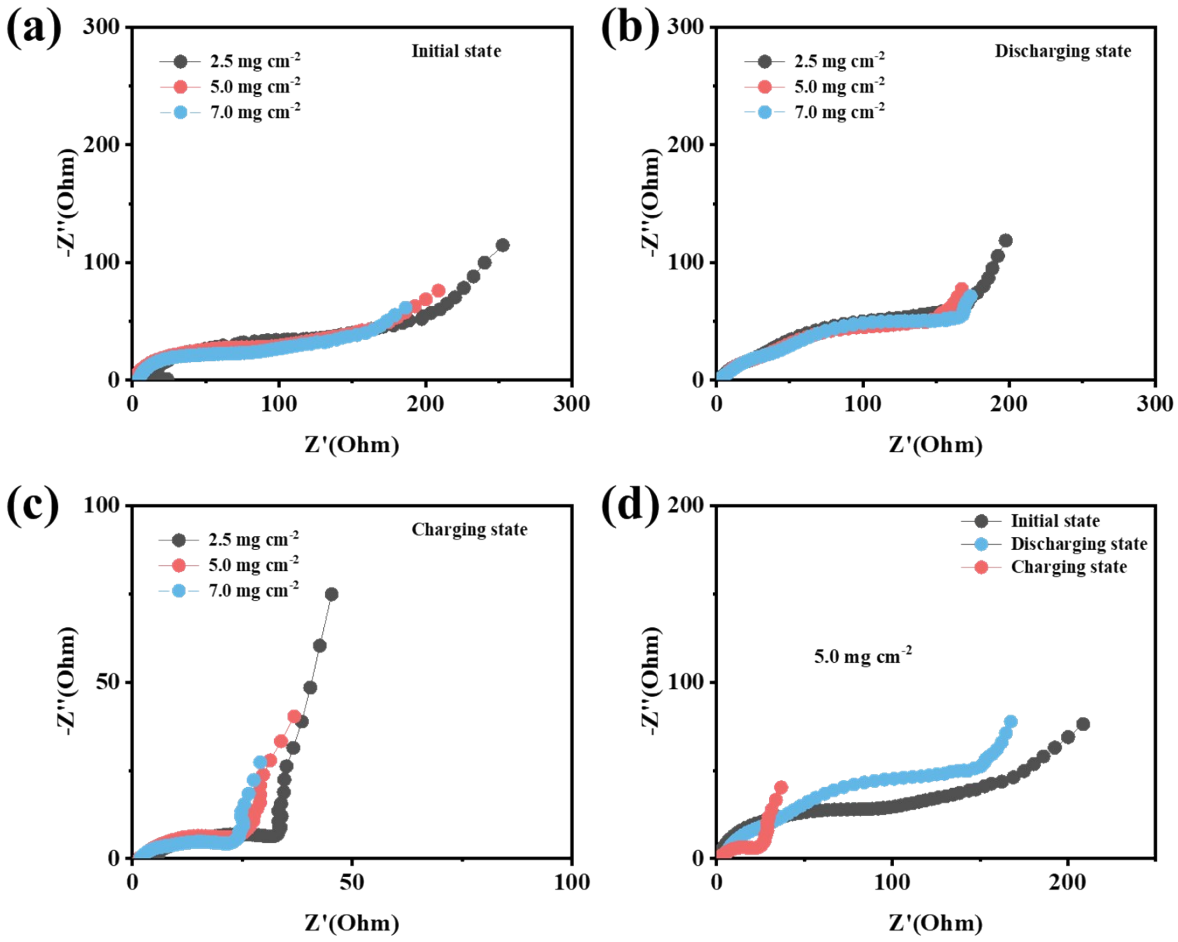

Figure S18. Nyquist plots of THC-based ZCC with several mass-loaded electrodes at different charge/discharge states (including initial state, discharging state (discharging to 0.1 V) and charging state (charging to 1.2 V)).

Note that the impedance changes of THC electrodes under different charging/discharging states may be related to surface byproducts caused by proton

mechanism. Please refer to the discussion of THC energy storage mechanism in the Manuscript.

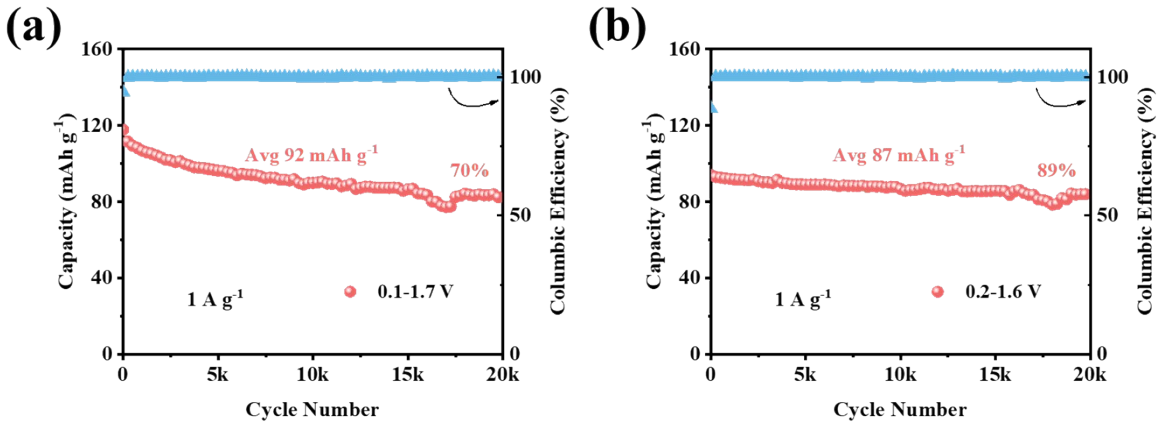

Figure S19. Long-cycle performance of THC-500 at 1 A g^{-1} (with the mass loading of 2-3 mg cm^{-2}).

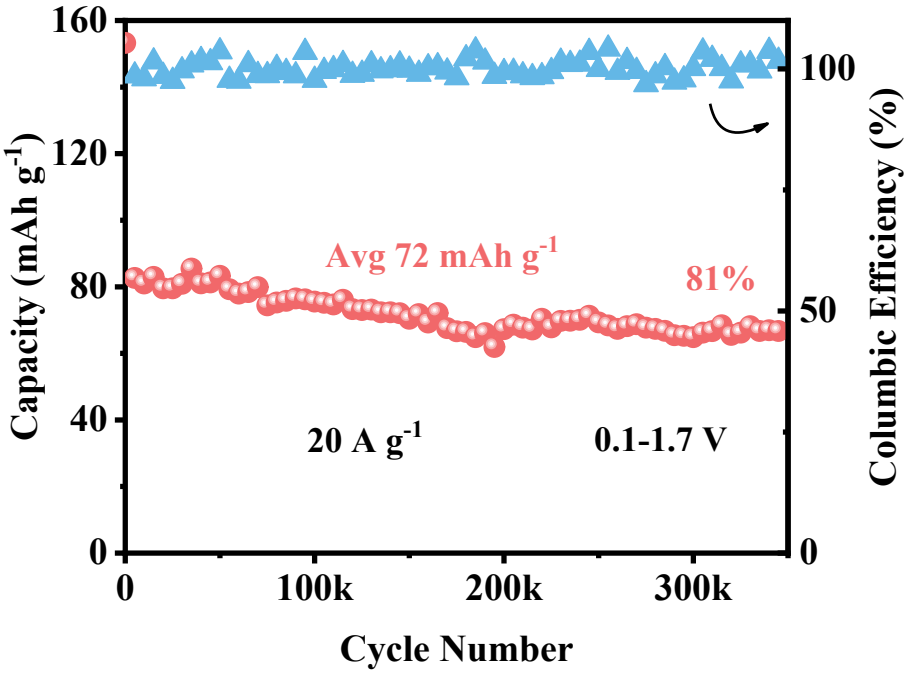

Figure S20. Long-cycle performance of THC-500 at 20 A g^{-1} (with the mass loading of 2-3 mg cm^{-2}).

Table S3.

(a). Comparison between THC-500 and reported carbon materials in terms of long cycle performance.

Ref	Mass loading [mg cm^{-2}]	Voltage [V]	Avg capacity[a]/Current density [mAh g^{-1}/A g^{-1}]	Cycle Number [k]	Cumulative capacity[b] [Ah g^{-1}]	Work time[c] [h]
THC-500	**2-3**	**0.1-1.7**	**~92/1**	**20**	**1,831**	**3,662**
			~76/5	**100**	**7,638**	**3,055**
			~72/20	**350**	**25,142**	**2,514**
		0.2-1.6	**~87/1**	**20**	**1,743**	**3,486**
			~71/5	**100**	**7,094**	**2,838**
SN-PCNTs[12]	0.7-0.8	0.2-1.8	~80/5	25	2,000	800
NAC[32]	2.5-3	0.2-1.8	~60/5	50	3,000	>50 days
N-OPCNF[33]	0.8-1.5	0.2-1.8	~60/40	200	12,000	600
WC-6ZnN-12U[13]	6	0.2-1.8	~70/2	50	3,500	3,500

NPC[14]	1.5	0-1.8	~75/10	60	4,500	900
N, S-PCD[29]	0.9	0.2-1.8	~100/5	100	10,000	>3,960 h
BNC[2]	1	0.05-1.8	~150/10	40	6,000	1,200
AC[34]	5	0.2-1.8	~50/2	15	750	>1 month
rGO-200[15]	1.2-1.5	0.01-1.8	~60/10	10	600	120
HPCS-900[17]	0.7-0.8	0.1-1.7	~45/10	30	1,350	270
AC[35]	/	0.2-1.85	~100/5	10	1,000	400
CT/SWNT-30[19]	2.7	0.2-1.8	~70/5	10	700	280
AC[20]	0.7-0.8	0.2-1.8	~80/1	10	800	1,600
NPG[22]	1.5	0-1.8	~50/10	15	750	300
OPCNF-20[23]	0.9-1.2	0.2-1.8	~55/5	50	2,750	1,100
OPC[24]	0.8-1.2	0.2-1.8	~70/1	10	700	1,400
CNPK[25]	1.77-2.12	0.2-1.8	~70/5	10	700	280
NPHC[36]	0.9	0.1-1.8	~70/5	20	1,400	560
NS-OPC[37]	1	0.01-1.8	~75/10	10	750	150
CTFO-NS-700[38]	1.5	0-2	~95/5	10	950	380
AC-SA[39]	1.9	0.15-	~70/45	300	21,000	930

		1.8				
HAPC[32, 40]	0.6	0.01-1.8	~100/10	18	1,800	360

[a] Average discharge capacity of long-cycle performance test. The avg capacity is estimated based on the long cycle performance data provided in the paper

[b] Cumulative capacity = Avg capacity × Cycle Number

[c] Unless the paper provides data, it is calculated according to the formula: Work time = Cumulative capacity × 2 / Current density

b. Comparison between THC-500 and reported non-carbon inorganic materials in terms of long cycle performance.

Ref	Mass loading [mg cm^{-2}]	Voltage [V]	Avg capacity[a]/Current density [mAh g^{-1}/A g^{-1}]	Cycle Number [k]	Cumulative capacity[b] [Ah g^{-1}]	Work time[c] [h]
THC-500	**2-3**	**0.1-1.7**	**~92/1**	**20**	**1,831**	**3,662**
			~76/5	**100**	**7,638**	**3,055**
			~72/20	**350**	**25,142**	**2,514**

		0.2-1.6	**~87/1**	**20**	**1,743**	**3,486**
			~71/5	**100**	**7,094**	**2,838**
$SeS_{5.76}$[41]	/	0.1-1.3	~650/4	0.5	325	163
VN[42]	0.6-0.7	0.3-1.9	~450/50	30	13,500	540
V_2O_3[43]	2	0.2-1.6	~500/10	10	5,000	1,000
MnO_2[44]	/	1.0-1.8	~60/1.855	10	600	637
FeHCF[45]	1.5-2	0.01-2.3	~65/3	10	650	433
MoS_2[46]	3.5	0.2-1.3	~110/2	1.5	165	165

[a] Average discharge capacity of long-cycle performance test. The avg capacity is estimated based on the long cycle performance data provided in the paper

[b] Cumulative capacity = Avg capacity × Cycle Number

[c] Unless the paper provides data, it is calculated according to the formula: Work time = Cumulative capacity × 2 / Current density

c. Comparison between THC-500 and reported non-carbon organic framework materials in terms of long cycle performance.

Ref	Mass loading [mg cm^{-2}]	Voltage [V]	Avg capacity[a]/Current density	Cycle Number	Cumulative capacity[b] [Ah g^{-1}]	Work time[c] [h]

			[mAh g^{-1}/A g^{-1}]	[k]		
			~92/1	**20**	**1,831**	**3,662**
		0.1-1.7	**~76/5**	**100**	**7,638**	**3,055**
THC-500	**2-3**		**~72/20**	**350**	**25,142**	**2,514**
			~87/1	**20**	**1,743**	**3,486**
		0.2-1.6	**~71/5**	**100**	**7,094**	**2,838**
PA-COF[47]	3	0.2-1.6	~130/1	10	1,300	2,600
Cu-BTA-H[48]	1.5	0.3-1.6	~130/2	0.5	65	65
HBOS[49]	3.2	0.5-1.5	~200/10	50	10,000	2,000
TA-PTO-COF[50]	1.0-1.1	0.3-1.7	~180/1	1	180	360

[a] Average discharge capacity of long-cycle performance test. The avg capacity is estimated based on the long cycle performance data provided in the paper

[b] Cumulative capacity = Avg capacity × Cycle Number

[c] Unless the paper provides data, it is calculated according to the formula: Work time = Cumulative capacity × 2 / Current density

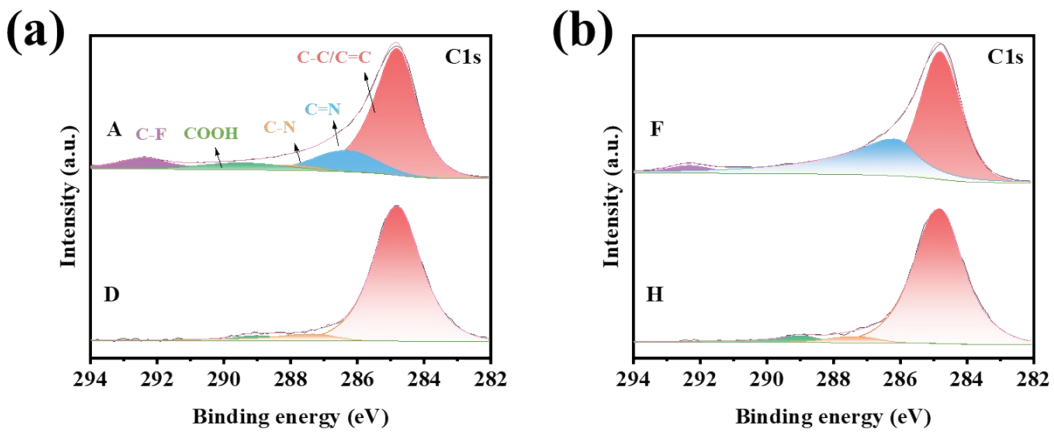

Figure S21. Ex-situ high-resolution C 1s spectra of THC-500 electrodes.

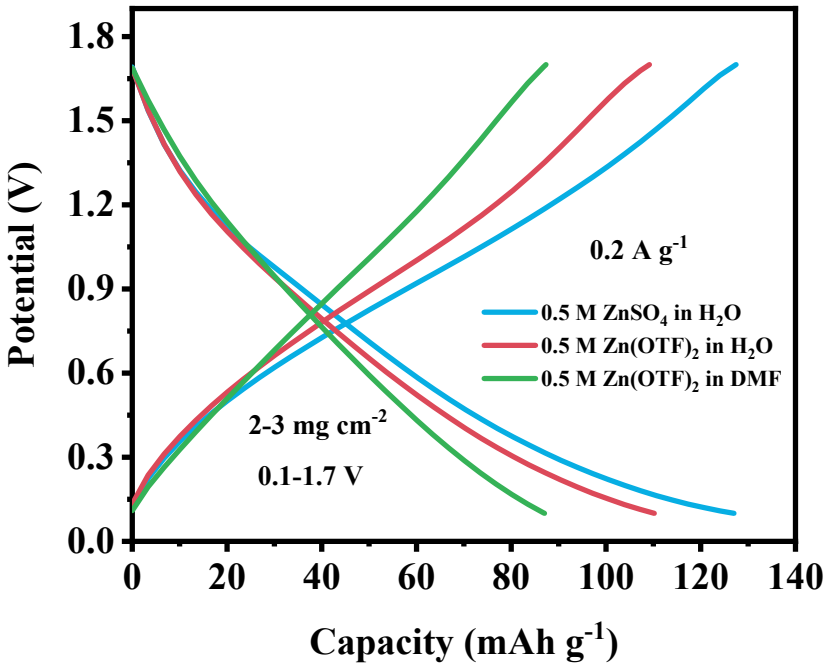

Figure S22. Galvanostatic charge-discharge curves of THC-500 in different electrolytes (including 0.5 M $Zn(OTF)_2$ in DMF, 0.5 M $Zn(OTF)_2$ in H_2O and 0.5 M $ZnSO_4$ in H_2O.

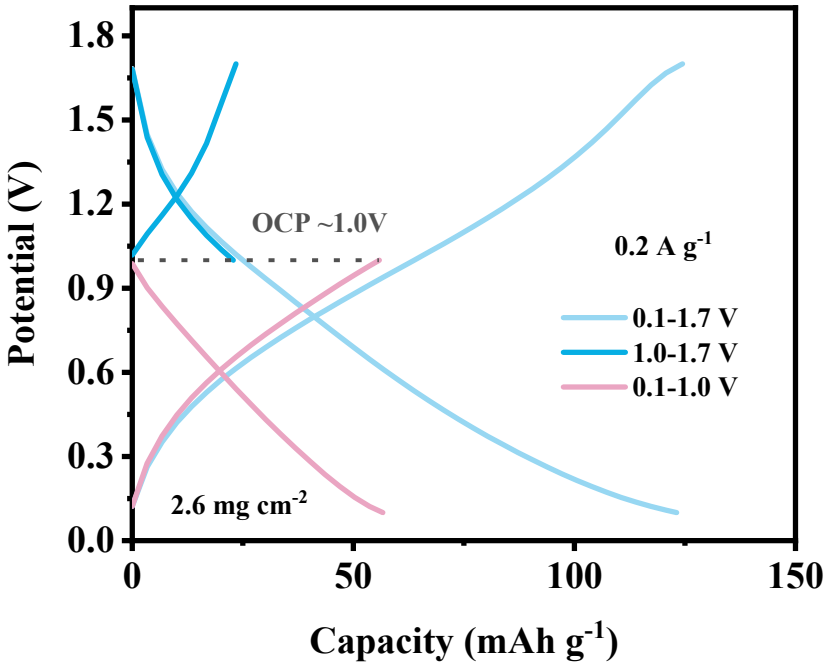

Figure S23. Galvanostatic charge-discharge curves of THC-based ZCC in different voltage ranges (the open-circuit potential (OCP) of ZCC is ~1.0 V vs. Zn^{2+}/Zn). The electrolyte is 2 M $ZnSO_4$ aqueous solution.

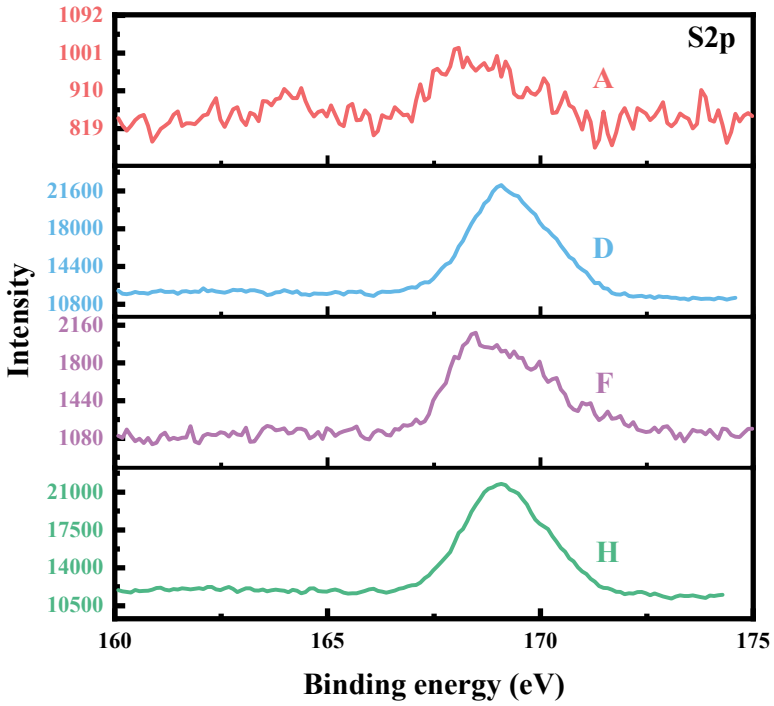

Figure S24. Ex-situ high-resolution XPS spectra of S 2p (the letter number of the electrodes charging/discharging states are consistent with **Figure 4a** in the manuscript).

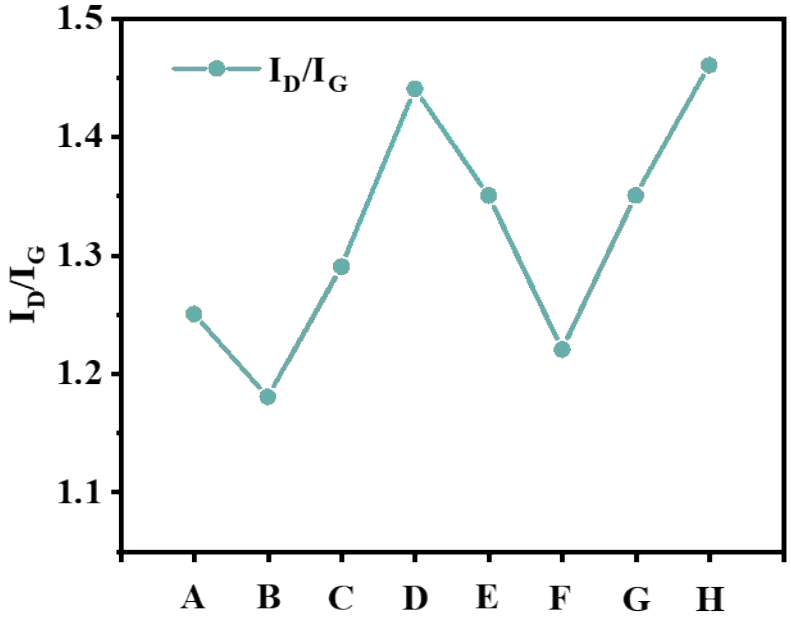

Figure S25. The corresponding I_D/I_G values of ex-situ Raman spectra.

References

1. P. Kuhn, M. Antonietti and A. Thomas, *Angew. Chem. Int. Ed.*, 2008, **47**, 3450-3453.
2. X. Chen, P. Ye, H. Wang, H. Huang, Y. Zhong and Y. Hu, *Adv. Funct. Mater.*, 2023, **33**, 2212915.
3. J. Ruan, F. Mo, Z. Chen, M. Liu, S. Zheng, R. Wu, F. Fang, Y. Song and D. Sun, *Adv. Energy Mater.*, 2020, **10**, 1904045.
4. J. Xu, F. Xu, M. Qian, F. Xu, Z. Hong and F. Huang, *Adv. Mater.*, 2017, **29**, 1701674.
5. F. Jiang, Y. Wang, T. Qiu, Y. Zhang, W. Zhu, C. Yang, J. Huang, Z. Fang and G. Dai, *ACS Appl. Mater. Interfaces*, 2021, **13**, 48818-48827.
6. W. Zhang, J. Yin, M. Sun, W. Wang, C. Chen, M. Altunkaya, A. H. Emwas, Y. Han, U. Schwingenschlogl and H. N. Alshareef, *Adv. Mater.*, 2020, **32**, e2000732.

7. F. Jiang, Y. Wang, T. Qiu, G. Yang, C. Yang, J. Huang, Z. Fang and J. Li, *J. Power Sources*, 2022, **523**, 231041.
8. M. Martin-Martinez, B. F. Machado, P. Serp, S. Morales-Torres, A. M. T. Silva, J. L. Figueiredo, J. L. Faria and H. T. Gomes, *Catal. Today*, 2020, **357**, 332-340.
9. Y. Zhao, S. Zhang, S. Xu, X. Li, Y. Zhang, Y. Xu, J. Zhou, H. Bi, F. Huang and T. Lin, *Macromol Rapid Commun*, 2022, **43**, 2200040.
10. B. Peng, Z. Lv, S. Xu, J. Pan, W. Zhao, C. Dong and F. Huang, *Adv. Mater.*, 2022, **34**, e2200863.
11. Z. Song, L. Miao, L. Ruhlmann, Y. Lv, D. Zhu, L. Li, L. Gan and M. Liu, *Adv. Mater.*, 2021, **33**, e2104148.
12. J. Li, L. Yu, W. Wang, X. He, G. Wang, R. Liu, X. Ma and G. Zhang, *J. Mater. Chem. A*, 2022, **10**, 9355-9362.
13. G. Lou, G. Pei, Y. Wu, Y. Lu, Y. Wu, X. Zhu, Y. Pang, Z. Shen, Q. Wu, S. Fu and H. Chen, *Chem. Eng. J.*, 2021, **413**, 127502.
14. X. Shi, H. Zhang, S. Zeng, J. Wang, X. Cao, X. Liu and X. Lu, *ACS Mater. Lett.*, 2021, **3**, 1291-1299.
15. H. Xu, W. He, Z. Li, J. Chi, J. Jiang, K. Huang, S. Li, G. Sun, H. Dou and X. Zhang, *Adv. Funct. Mater.*, 2022, **32**, 2111131.
16. W. Jian, W. Zhang, B. Wu, X. Wei, W. Liang, X. Zhang, F. Wen, L. Zhao, J. Yin, K. Lu and X. Qiu, *ACS Appl. Mater. Interfaces*, 2022, **14**, 5425-5438.
17. K. Shang, Y. Liu, P. Cai, K. Li and Z. Wen, *J. Mater. Chem. A*, 2022, **10**, 6489-6498.
18. L. Zhao, W. Jian, J. Zhu, X. Zhang, F. Wen, X. Fei, L. Chen, S. Huang, J. Yin, N. R. Chodankar, X. Qiu and W. Zhang, *ACS Applied Materials & Interfaces*, 2022, **14**, 43431-43441.
19. Y. Cao, X. Tang, M. Liu, Y. Zhang, T. Yang, Z. Yang, Y. Yu, Y. Li, J. Di and Q. Li, *Chem. Eng. J.*, 2022, **431**, 133241.
20. L. Dong, X. Ma, Y. Li, L. Zhao, W. Liu, J. Cheng, C. Xu, B. Li, Q.-H. Yang and F. Kang, *Energy Stor. Mater.*, 2018, **13**, 96-102.
21. Y. Zhang, Z. Wang, D. Li, Q. Sun, K. Lai, K. Li, Q. Yuan, X. Liu and L. Ci, *J. Mater. Chem. A*, 2020, **8**, 22874-22885.
22. Y. Zhao, H. Hao, T. Song, X. Wang, C. Li and W. Li, *J. Power Sources*, 2022, **521**, 230941.
23. H. He, J. Lian, C. Chen, Q. Xiong and M. Zhang, *Chem. Eng. J.*, 2021, **421**, 129786.
24. Y. Zheng, W. Zhao, D. Jia, Y. Liu, L. Cui, D. Wei, R. Zheng and J. Liu, *Chem. Eng. J.*, 2020, **387**, 124161.
25. H. Zhang, Z. Chen, Y. Zhang, Z. Ma, Y. Zhang, L. Bai and L. Sun, *J. Mater. Chem. A*, 2021, **9**, 16565-16574.
26. Y. Lu, Z. Li, Z. Bai, H. Mi, C. Ji, H. Pang, C. Yu and J. Qiu, *Nano Energy*, 2019, **66**, 104132.
27. Y. Zhu, X. Ye, H. Jiang, J. Xia, Z. Yue, L. Wang, Z. Wan, C. Jia and X. Yao, *J. Power Sources*, 2020, **453**, 227851.

28. W. Jian, W. Zhang, X. Wei, B. Wu, W. Liang, Y. Wu, J. Yin, K. Lu, Y. Chen, H. N. Alshareef and X. Qiu, *Adv. Funct. Mater.*, 2022, **32**, 2209914.
29. Y. Yang, D. Chen, H. Wang, P. Ye, Z. Ping, J. Ning, Y. Zhong and Y. Hu, *Chem. Eng. J.*, 2022, **431**, 133250.
30. L. Zhao, W. Jian, J. Zhu, X. Zhang, F. Wen, X. Fei, L. Chen, S. Huang, J. Yin, N. R. Chodankar, X. Qiu and W. Zhang, *ACS Appl. Mater. Interfaces*, 2022, **14**, 43431-43441.
31. Y. Zhang, S. Zhang, Z. Chen, T. Li, Y. Zhao, F. Huang and T. Lin, *J. Mater. Chem. A*, 2022, **10**, 9402-9407.
32. N. Chang, T. Li, R. Li, S. Wang, Y. Yin, H. Zhang and X. Li, *Energy Environ. Sci.*, 2020, **13**, 3527-3535.
33. H. He, J. Lian, C. Chen, Q. Xiong, C. C. Li and M. Zhang, *Nanomicro Lett*, 2022, **14**, 106.
34. P. Xiong, Y. Kang, N. Yao, X. Chen, H. Mao, W.-S. Jang, D. M. Halat, Z.-H. Fu, M.-H. Jung, H. Y. Jeong, Y.-M. Kim, J. A. Reimer, Q. Zhang and H. S. Park, *ACS Energy Lett.*, 2023, DOI: 10.1021/acsenergylett.3c00154, 1613-1625.
35. P. Wang, X. Xie, Z. Xing, X. Chen, G. Fang, B. Lu, J. Zhou, S. Liang and H. J. Fan, *Adv. Energy Mater.*, 2021, **11**, 2101158.
36. H. Peng, X. Wang, Z. Liu, H. Lei, S. Cui, X. Xie, Y. Hu and G. Ma, *ACS Appl. Mater. Interfaces*, 2023, **15**, 4071-4080.
37. J. Yu, X. Jia, J. Peng, B. Meng, Y. Wei, X. Hou, J. Zhao, N. Yang, K. Xie, D. Chu and L. Li, *ACS Appl. Energy Mater.*, 2023, **6**, 2728–2738.
38. B. Liu, T. Quan, M. Yang, Y. Liu, H. Chen and H. Li, *Chem. Eng. J.*, 2023, **461**, 141925.
39. Z. Xu, R. Ma and X. Wang, *Energy Stor. Mater.*, 2022, **46**, 233-242.
40. Z. Zhou, X. Zhou, M. Zhang, S. Mu, Q. Liu and Y. Tang, *Small*, 2020, **16**, e2003174.
41. W. Li, Y. Ma, P. Li, X. Jing, K. Jiang and D. Wang, *Adv. Funct. Mater.*, 2021, **31**, 2101237.
42. Y. Zhang, S. Jiang, Y. Li, X. Ren, P. Zhang, L. Sun and H. Y. Yang, *Adv. Energy Mater.*, 2022, **13**, 2202826.
43. H. Luo, B. Wang, F. Wang, J. Yang, F. Wu, Y. Ning, Y. Zhou, D. Wang, H. Liu and S. Dou, *ACS Nano*, 2020, **14**, 7328-7337.
44. W. Sun, F. Wang, S. Hou, C. Yang, X. Fan, Z. Ma, T. Gao, F. Han, R. Hu, M. Zhu and C. Wang, *Journal of the American Chemical Society*, 2017, **139**, 9775-9778.
45. Q. Yang, F. Mo, Z. Liu, L. Ma, X. Li, D. Fang, S. Chen, S. Zhang and C. Zhi, *Advanced Materials*, 2019, DOI: 10.1002/adma.201901521.
46. H. Liu, J.-G. Wang, W. Hua, Z. You, Z. Hou, J. Yang, C. Wei and F. Kang, *Energy Stor. Mater.*, 2021, **35**, 731-738.
47. W. Wang, V. S. Kale, Z. Cao, S. Kandambeth, W. Zhang, J. Ming, P. T. Parvatkar, E. Abou-Hamad, O. Shekhah, L. Cavallo, M. Eddaoudi and H. N. Alshareef, *ACS Energy Lett.*, 2020, **5**, 2256-2264.

48. Z. Sang, J. Liu, X. Zhang, L. Yin, F. Hou and J. Liang, *ACS Nano*, 2023, **17**, 3077-3087.
49. Z. Song, L. Miao, L. Ruhlmann, Y. Lv, L. Li, L. Gan and M. Liu, *Angew. Chem. Int. Ed.*, 2023, **62**, e202219136.
50. H. Li, M. Cao, Z. Fu, Q. Ma, L. Zhang, R. Wang, F. Liang, T. Zhou and C. Zhang, *Chem. Sci.*, 2024, DOI: 10.1039/d3sc07013a.